Hindawi
Shock and Vibration
Volume 2023, Article ID 5553183, 19 pages
https://doi.org/10.1155/2023/5553183

Research Article

Influence of Fir-Tree Tenon Blade Parameters on Blade Dynamic Characteristics

Zhenya Yang[1] and Chaofeng Li[1,2]

[1]*School of Mechanical Engineering and Automation, Northeastern University, Shenyang, Liaoning 110819, China*
[2]*Key Laboratory of Vibration and Control of Aero-Propulsion Systems, Ministry of Education of China, Northeastern University, Shenyang, Liaoning 110819, China*

Correspondence should be addressed to Chaofeng Li; chfli@mail.neu.edu.cn

Received 5 December 2022; Revised 30 May 2023; Accepted 2 June 2023; Published 17 June 2023

Academic Editor: Dario Di Maio

In this paper, based on the theory of elastic structure analysis, considering the rotational softening and centrifugal stiffening of the blade, the dynamic model of the fir-tree rotating blade and the macroslip hysteresis model of the dry friction on the contact surface of fir-tree tenon are established. Based on elastic mechanics, the pressure distribution model of fir-tree tenon is innovatively established and the relationship between fit clearance and contact pressure has been derived. After the blade is discretized by the finite element method, the dynamic equation of the blade is solved iteratively by the Newmark-β numerical integration method. According to the dynamic equation of the blade, the influence of the change of the tenon angle on the forced response and contact stress of the blade is derived. Finally, some novel conclusions are obtained by analyzing the influence of pressure distribution, tenon angle, friction coefficient, rotational speed, and aerodynamic excitation on blade vibration characteristics. It provides a scheme and relevant basis for the design and development of tenon blades with the most damping effect at different speeds in industrial practice.

1. Introduction

A blade is an important component of turbomachinery such as aeroengine and turbine. The quality and structure of a blade will directly affect the performance, reliability, and life of turbomachinery. According to statistics, engine failure caused by blade fatigue fracture accounts for more than half of the causes of engine failure. The fatigue fracture of the blade is sudden, which causes most of the faults of the blade to bring huge economic losses and even casualties. Therefore, it is necessary to prevent the fatigue failure of the blade in industrial practice. Because one of the main causes of blade fatigue failure is the alternating stress in the blade, in recent decades, many scholars and manufacturers in high performance impeller machinery are very concerned about the vibration reduction of the blade to prevent fatigue cracks and even fractures [1–4]. In order to reduce the alternating stress in the blade and reduce the high cycle fatigue damage of the blade, it is a simple and effective way to reduce the vibration level of the blade by using the friction energy dissipation between the contact surfaces of the tenon joint structure. Therefore, the design of a tenon structure with good vibration damping to maximize its effectiveness in operation and the establishment of an accurate and efficient dynamics model are essential tasks in the design and study of tenon blades [5, 6].

Zucca et al. [7] proposed a method for calculating the friction force on the contact surface during blade vibration. Considering the local contact characteristics, the dynamic equation of the dovetail tenon blade was established. Chen et al. [8] established the contact slip mechanical model considering the distribution characteristics of contact pressure and applied it to the dovetail tenon root. The dynamic equation of the blade was obtained by the finite element method. Finally, the harmonic balance method was used to solve the dynamic equation, and the accuracy and

universality of the model were verified. Based on the finite element theory, Li et al. [9] established the finite element model of a flexible dovetail blade by using the space beam element. Through the change of friction and dry friction energy dissipation ratio in the process of blade vibration, the vibration reduction mechanism of the blade with dovetail root was expounded. Li et al. [10] established a macroslip friction model at the dovetail tenon root. On this basis, the linearization of nonlinear friction was realized, and the vibration response of the blade was calculated by the time domain method. Chen et al. [11] used 2D and 3D friction contact models to numerically study the friction damping effect on the root contact surface of the dovetail blade. The hysteresis curves of the tenon root under different modeling parameters were analyzed, and the effects of physical parameters such as geometric parameters, friction coefficient, contact stiffness, and tangential and normal load on friction damping effect were studied. Wang et al. [12] established the dynamic model of dovetail tenon blade, using spring and viscous damper to describe the normal pressure on the contact surface. The effects of contact stiffness, contact damping, and rotational speed on the dynamic characteristics of the blade are analyzed. She et al. [13] developed a continuum model of a wheel-dovetail beam and investigated the coupled vibration mechanism of the system by employing macroslip dry friction theory. Ma et al. [14] established the finite element model of dovetail blade-disc and analyzed the influence of rotational speed and invasion depth on blade vibration response and root contact behavior under blade tip rubbing conditions. Lemoine et al. [15] proposed a calculation method combining the HBM and the DLFT and analyzed the dynamic response of the dovetail tenon blade under different friction coefficients and excitation levels. The change of contact force and contact behavior of the middle node of the contact surface was studied. Asia et al. [16] studied the root-damping effect of the dovetail tenon structure. The effects of installation angle and centrifugal load on damping ratio and natural frequency were discussed, and the effects of loading times and specimen geometry on tangential stiffness were analyzed. Huels et al. [17] established the finite element model of the tenon-connected turbine blade and analyzed the influence of the basic geometric design parameters of the blade on the nonlinear vibration response of the blade. Li et al. [18] established the dynamic model of dovetail blade based on the finite element method and used the dry friction macroslip model to simulate the contact surface friction force. The nonlinear dynamics of dovetail blade was studied. Li et al. [19] established the finite element model of dovetail blade and used the one-dimensional dry friction model to capture the mechanical characteristics of the contact interface. The influence of tenon structure parameters on the vibration characteristics of the blade was studied.

With the in-depth study of tenon-joint friction damper, scholars have found that although the dovetail tenon-joint friction damper has a significant indigenous effect on the vibration reduction of the blade, it also has the following shortcomings: (1) as only one pair of contact surfaces are in play in the dovetail construction, the stresses on the individual contact surfaces are higher. (2) In order to ensure the strength of the tenon joint, the circumferential dimensions and weight of the tenon root are relatively large. (3) The dovetail tenon structure can only play the role of friction damping when the rotational speed is low, and the damping effect is lost when the rotational speed is high. However, the fir-tree tenon structure not only overcomes the disadvantages of the dovetail construction but also allows for a larger gap between the tenon and the nonsupporting surface of the tenon groove, into which cold air can be passed for cooling, while more blades can be fitted due to the small circumferential size of the tenon. As a result, many scholars have turned their attention to the fir-tree tenon structure. Petrov and Ewins [20] studied the forced vibration response of a fir-tree tenon structure. A surface friction contact element was introduced in the contact area of the tenon, and the relationship between the friction damping at the root of the blade and the response amplitude of the blade was analyzed. Meguid et al. [21] carried out two-dimensional and three-dimensional finite element analysis on the fir-tree tenon root and pointed out that the three-dimensional calculation could accurately obtain the stress distribution in the blade root rim area, and discussed the influence of design size on the blade root rim strength. Lavella and Botto [22] convert the centrifugal load of the blade to the tooth surface of the tenon and tenon groove equally when calculating the stresses in the blade and the wheel disc, while cutting down the root and the tooth groove for separate analysis when calculating the contact stresses in the tenon and tooth area, loading the centrifugal force of the blade to the upper surface of the root equally. Koscso and Petrov [23] investigated nonlinear contact interactions at the leaf roots through high-fidelity modeling of fir-tree tenon-and-groove bladed disc assemblies and nonlinear contact modeling of bladed disc contact blocks, analyzing the effects of the number, location, and distribution of nonlinear contact elements and finding that small differences in root geometry lead to significant changes in the nonlinear forcing response. Ferhatoglu and Zucca [24] proposed a numerical method for determining the variation range periodic response boundaries for all fir-tree turbine blades with frictional damping and a large number of contacts. The system's damping loss factor was used as the objective function to minimize while satisfying the harmonic balance method (HBM), resulting in a system of nonlinear algebraic equations. Zhao et al. [25] established a two-dimensional friction model considering the variation of normal force with excitation at the tenon-and-groove

contact surface, investigated the effect of variable normal vibration on the blade response, and analyzed the effect of detuning of blade parameters such as the tangential stiffness of the friction surface and structural stiffness on the coupled vibration. Shukla and Harsha [26] used the finite element method to develop a mathematical model of a fir-tree blade, on the basis of which the blade was analyzed and compared with experiments to verify the correctness of the model and the reliability of the response results. Shukla and Harsha [27] established the finite element model of the fir-tree tenon blade and studied the influence of different size cracks on the vibration characteristics of the blade by adjusting the size of the root crack. The correctness of the finite element model was verified by comparing the analysis results with the experiment. Zucca et al. [28] established a finite element model of a fir-tree tenon blade with a pin damper. After the matrix was simplified by CB-CMS, the blade response was calculated based on the harmonic balance method. The effects of three different types of dampers, cylindrical, asymmetric, and wedge-shaped on the vibration characteristics of blades were analyzed. Through experimental comparison, it was found that the performance of asymmetric dampers was the best. Quaegebeur et al. [29] considered the centrifugal effect and the friction and separation of the tenon joint structure and established the finite element model of the fir-tree tenon blade with platform damper. The finite element model was reduced by combining the nonlinear identification of the interaction nodes with the linear component mode. The dynamic Lagrangian frequency time algorithm was used to analyze the vibration characteristics of the blade. Petrov [30] established the dry friction model of the fir-tree tenon structure through the surface friction contact element. The dynamic equation of the blade was established by the finite element method. Krack et al. [31] established the fir-tree tenon blade model with shroud and flange damper by considering microslip and aeroelastic effects. After model reduction, the blade's forced vibration and self-excited vibration were calculated and analyzed by the higher harmonic balance method. Koscso and Petrov [32] established the finite element model of a fir-tree tenon blade with shroud and studied the vibration characteristics of an anisotropic mistuned blade by the harmonic balance method. Chen et al. [33] established a large finite element model of the fir-tree tenon structure. A large number of face-to-face elements were used to simulate and capture the microslip phenomenon and action on the tenon contact surface. The effects of the modal damping factor and blade modal shape on the vibration response were studied and analyzed.

In recent years, the research on the tenon joint structure has almost always been to improve the contact model or use the high degree of freedom model to improve the accuracy. However, the influence of the contact pressure change of the tenon structure on the vibration characteristics of the blade was not considered. In previous studies, the pressure on the contact surface of the fir-tree tenon was evenly distributed to three pairs of surfaces, without considering the diversity of pressure ratio caused by assembly and other problems in industrial practice. Moreover, the intermittent excitation was almost used in the dynamic analysis of blades, without considering the influence of actual aerodynamic excitation on the dynamic characteristics of blades.

In this paper, based on the theory of elastic structure analysis, considering the bending, shearing, rotating softening, and centrifugal stiffening of rotating blades, the dynamic model of the fir-tree rotating blades is established. Based on the macroslip hysteresis model of the Coulomb friction theorem, the dry friction mechanical model is established on the contact surface of the fir-tree tenon. Under certain conditions, the mathematical expression that should be satisfied between the positive pressure and fitting clearance on the contact surface of the fir-tree tenon is innovatively proposed. According to the principle of force balance and the geometric relationship of the blade, different distribution modes of positive pressure on the contact surface of the tenon root are obtained. The effects of pressure distribution, tenon angle, friction coefficient, rotation speed, and aerodynamic excitation on blade vibration characteristics are studied. It provides a scheme and related theoretical basis for the design and development of tenon blades with the most damping effect at different speeds in industrial practice.

2. Blade Dynamics Model

As a key component in rotating machinery such as gas turbines, a blade should have sufficient stiffness and the ability to resist external excitation and suppress vibration. The fir-tree tenon structure is widely used because of its high strength, small size, and lightweight. Considering the complexity of the fir-tree tenon blade and the non-negligible height-span ratio, the finite element model of the shear coupled bending fir-tree tenon blade in a rotating state is established based on the theory of elastic structure analysis. The finite element model of the blade is shown in Figure 1.Here, *oxyz* is the local coordinate system of the blade. The parameters of the finite element model of the blade are shown in Table 1.

Based on the established finite element model, the dynamic model of the blade is established using elastic mechanics and energy theory. The energy Q^e of each element of the rotating blade under harmonic excitation can be expressed by the following equation:

$$Q^e = U_b^e + U_s^e + U_c^e + T_b^e + T_s^e, \tag{1}$$

where U_b^e is the strain energy caused by the bending deformation of the element, U_s^e is the strain energy caused by the shear deformation of the element, U_c^e is the centrifugal strain energy of the element, T_b^e is the kinetic energy caused by the bending deformation of the element, and T_s^e is the kinetic energy caused by the shear deformation of the element.

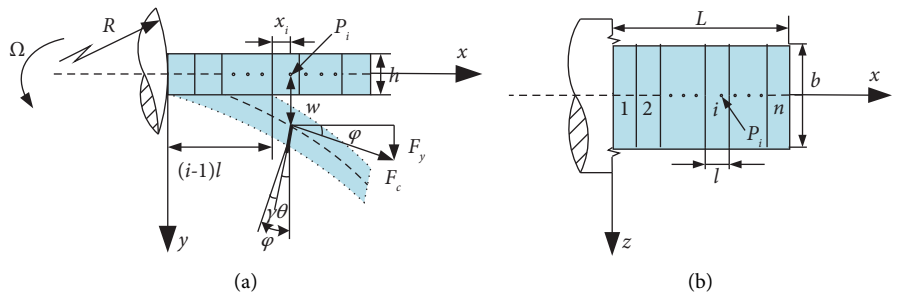

Figure 1: The finite element model of the blade.

Table 1: The parameters of the finite element model.

Symbols	Meaning	Unit
Ω	The rotational speed of the system	rad/s
R	Blade disc radius	mm
L	Length of the blade	mm
B	Width of the blade	mm
H	Height of the blade	mm
n	Number of the blade division elements	—
$l = L/n$	Length of the element	mm
P_i	Any point in the i-th element	—
x_i	Distance from P_i to the first node of the i-th element	mm
E	Young's modulus of the blade	Pa
υ	Poisson's ratio of the blade	—
I	Moment of inertia of the blade section	mm^4
ρ	The density of the blade	kg/m^3
κ	Shear correction factor	—
w	Lateral displacement due to blade deformation	mm
F_c	The centrifugal force of the blade	N
F_y	Lateral component of centrifugal force	N
γ	Shear strain due to shear force	—
Θ	The rotation angle of the blade section	°
φ	Neutral shaft angle	°

In the local coordinate system $oxyz$, each of the potential and kinetic energies in equation (1) can be expressed separately in the following equation:

$$\begin{cases} U_b^e = \dfrac{1}{2}\displaystyle\int_{(i-1)l}^{il} \mathrm{EI}\left(\frac{\partial^2 \omega_b^e}{\partial x^2}\right)^2 \mathrm{d}x, \\ U_s^e = \dfrac{1}{2}\displaystyle\int_{(i-1)l}^{il} \frac{\mathrm{GA}}{\kappa}\left(\frac{\partial \omega_s^e}{\partial x}\right)^2 \mathrm{d}x, \\ U_c^e = \dfrac{1}{2}\displaystyle\int_{(i-1)l}^{il} F_c^e\left(\frac{\partial \omega}{\partial x}\right)^2 \mathrm{d}x, \\ T_b^e = \dfrac{1}{2}\displaystyle\int_{(i-1)l}^{il} \rho A\left(\frac{\partial \omega_b^e}{\partial t}\right)^2 \mathrm{d}x, \\ T_s^e = \dfrac{1}{2}\displaystyle\int_{(i-1)l}^{il} \rho A\left(\frac{\partial \omega_s^e}{\partial t}\right)^2 \mathrm{d}x, \end{cases} \tag{2}$$

where ω_b^e and ω_s^e are the displacements caused by the bending deformation and shear deformation of the blade, respectively.

Considering the general expressions of element strain energy and kinetic energy and combining them with equation (2), element bending stiffness matrix $\mathbf{k}_b^e$, element shear stiffness matrix $\mathbf{k}_s^e$, element centrifugal stiffness matrix $\mathbf{k}_c^e$, and element mass matrices $\mathbf{m}_b^e$ and $\mathbf{m}_s^e$ can be obtained. The whole mass matrix $\mathbf{M}$ and stiffness matrix $\mathbf{K}$ of the blade system are obtained by converting the element matrices in the local coordinate system to the whole coordinate system.

The size of the damping determines the nature of the vibration of the system. In this paper, alpha-beta damping, also known as Rayleigh damping, is used as the damping of the system in combination with several damping forms commonly used in engineering. Its form can be expressed by the following equation:

$$\mathbf{C} = \lambda_1 \mathbf{M} + \lambda_2 \mathbf{K}, \tag{3}$$

where $\mathbf{M}$ and $\mathbf{K}$ are the overall mass and stiffness matrices of the system, while λ_1 and λ_2 are the mass and stiffness damping coefficients, respectively. The values of λ_1 and λ_2 can be determined by determining the two-order modal damping ratios and the inherent frequencies, which are expressed as follows:

$$\begin{cases} \lambda_1 = 2\dfrac{(\xi_2/\omega_2) - (\xi_1/\omega_1)}{(1/\omega_2^2) - (1/\omega_1^2)} = 2\dfrac{\omega_1\omega_2(\xi_1\omega_2 - \xi_2\omega_1)}{\omega_2^2 - \omega_1^2}, \\ \lambda_2 = 2\dfrac{\xi_2\omega_2 - \xi_1\omega_2}{\omega_2^2 - \omega_1^2}. \end{cases} \tag{4}$$

In equation (4), ω_1 and ω_2 are the first two inherent frequencies of the system and ξ_1 and ξ_2 are the modal damping ratios corresponding to the first two inherent frequencies, respectively.

According to the mass matrix, stiffness matrix, and damping matrix of the blade, the finite element dynamic equation of the blade is established. The expression is as follows:

$$\mathbf{M}\ddot{\mathbf{X}} + \mathbf{C}\dot{\mathbf{X}} + \mathbf{K}\mathbf{X} = \mathbf{Q} - \mathbf{F}, \tag{5}$$

where $\mathbf{Q}$ is the external excitation acting on the blade and $\mathbf{F}$ is the damping force generated by the tenon damper.

3. Dry Friction Model and Pressure Ratio Model

3.1. Dry Friction Model. When the fir-tree tenon blade is working, the tenon root of the blade will be closely bonded with the wheel disc due to the centrifugal force so that the blade will be positioned on the wheel disc rotor. There is not only positive pressure due to centrifugal force but also dry friction due to blade vibration on the contact surface between the tenon and wheel disc. The dry friction of the contact surface can consume the energy of the blade vibration to reduce the blade vibration. However, the dry friction forces acting on the blade root surface are very complex and in order to facilitate the description of the nonlinear dry friction forces, the following assumptions are made in this paper:

(1) It is assumed that the blade tenon root never separates from the wheel disc during operation

(2) It is assumed that the positive pressure on the contact surface between the tenon root and the wheel disc remains constant throughout the vibration of the blade

(3) It is assumed that the contact angle of the tenon root remains constant during the vibration of the blade and that the blade only moves horizontally

Using artificial springs to simulate the boundary conditions of the model is a common method to deal with boundary problems [34, 35]. Under the abovementioned assumptions, the dry friction model is established as shown in Figure 2. The model simplifies the blade root to an ideal dry friction damper with massless and flexible. The specific parameters of the dry friction model are shown in Table 2, where $i = 1, 2, 3$; $j = 1, 2$.

Since the tenon root only moves horizontally $y(t)$, equation (6) can be obtained according to the geometric relationship.

$$\begin{cases} d_{i1} \cos a_i = y(t), \\ d_{i2} \cos \beta_i = y(t). \end{cases} \tag{6}$$

The contact interface friction depends on the relationship between the spring force $k_{ij}(d_{ij} - w_{ij})$ and the maximum static friction force $\mu_{ij} N_{ij}$. When the spring force is less than the maximum static friction force, the contact surfaces will stick to each other and the friction force is equal to the spring force. When the spring force is greater than the maximum static friction force, the contact surface will slip between each other and the friction force is equal to the maximum static friction force. The expression is as follows:

$$f_{ij} = \begin{cases} k_{ij}\left(d_{ij} - w_{ij}\right), & k_{ij}\left|d_{ij} - w_{ij}\right| \le \mu_{ij} N_{ij}, \\ \mu_{ij} N_{ij} sgn\left(\dot{w}_{ij}\right), & k_{ij}\left|d_{ij} - w_{ij}\right| > \mu_{ij} N_{ij}. \end{cases} \tag{7}$$

According to the equilibrium condition of force and ignoring the influence of friction on the contact surface, the positive pressure on each contact surface can be expressed as follows:

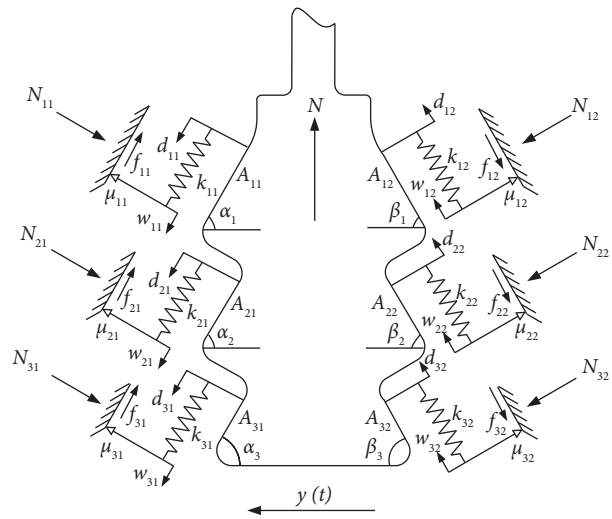

Figure 2: The dry friction model of fir-tree tenon structure.

$$\begin{cases} N_{i1} = \dfrac{N_i \sin \beta_i}{\sin\left(\alpha_i + \beta_i\right)}, \\ N_{i2} = \dfrac{N_i \sin \alpha_i}{\sin\left(\alpha_i + \beta_i\right)}, \end{cases} \tag{8}$$

where N_i is the component of the positive pressure on the i-th pair of contact surfaces in the radial direction. N_i and the centrifugal force N satisfy the following equation:

$$N = \sum_{i=1}^{3} N_i. \tag{9}$$

According to the centrifugal force calculation formula and the blade parameters, it is easy to obtain that the centrifugal force N of the blade is as follows:

$$N = \int_{R}^{R+L} \rho A \Omega^2 x \mathrm{d}x. \tag{10}$$

The friction f_{ij} on the contact surface of the tenon is projected in the horizontal direction to obtain the component of the dry friction in the horizontal direction. The expression is as follows:

$$f_n = \sum_{i=1}^{3} \left(f_{i1} \cos \alpha_i + f_{i2} \cos \beta_i\right). \tag{11}$$

3.2. Pressure Ratio Model. The small change of the fitting clearance between the tenon root and the tenon groove in the fir-tree tenon joint structure will cause a great change in the positive pressure on the three pairs of contact surfaces and then affect the nonlinear friction force on the contact surface of the tenon joint structure. Therefore, it is necessary to establish the contact model of the relationship between positive pressure and fitting clearance to realize the adjustable distribution of pressure. In order to describe the

Table 2: The parameters of the fir-tree tenon structure.

Symbols	Meaning	Unit
N	Centrifugal force on the blade	N
N_{ij}	Positive pressure generated by N on the i-th pair of contact surfaces j	N
$y\ (t)$	Displacement of blade roots in the horizontal direction	mm
d_{ij}	Displacement of x on the tangent of the i-th pair of contact surfaces j	mm
α_i	The angle between the i-th pair of contact surfaces 1 and the horizontal direction	°
β_i	The angle between the i-th pair of contact surfaces 2 and the horizontal direction	°
A_{ij}	The surface area of the i-th pair of contact surfaces j	mm^2
w_{ij}	Displacement of the friction dampers on the i-th pair of contact surfaces j	mm
k_{ij}	Coefficient of shear stiffness on the i-th pair of contact surfaces j	N/mm
μ_{ij}	Coefficient of friction on the i-th pair of contact surfaces j	—
f_{ij}	Friction on the i-th pair of contact surfaces j	N

relationship between positive pressure and fitting clearance, this paper makes the following assumptions:

(1) It is assumed that the positive pressure on the three pairs of contact surfaces remains unchanged during the vibration of the blade

(2) It is assumed that the three pairs of contact surfaces of the blade are in contact and there is a constant contact pressure during the vibration process

(3) It is assumed that the deformation process between the tenon root and the tenon groove interface is an elastic deformation process during the vibration of the blade

The fir-tree tenon contact model is shown in Figure 3, where δ_1, δ_2, and δ_3 are the fitting clearances between the tenon root and tenon groove when the blade is static.

Assuming that the first pair of contact surfaces is the main bearing surface during vibration, the contact pressure N_i on the three pairs of contact surfaces can be expressed by the following equation:

$$N_i = \begin{cases} k\Delta, \\ k(\Delta - \Delta x_2), \\ k(\Delta - \Delta x_3), \end{cases} \tag{12}$$

where Δ is the amount of deformation of the main bearing surface under contact pressure N_1, Δx_2, and Δx_3 are the gap between the second pair of contact surfaces and the gap between the third pair of contact surfaces, respectively, when the main bearing surfaces first come into contact. k is the contact stiffness of the tenon structure. In this paper, the first item of the overall stiffness matrix is taken as the contact stiffness of the tenon structure.

The pressure on the three pairs of contact surfaces of the fir-tree tenon structure is N_1, N_2, and N_3, respectively. By solving equation (12), when the contact pressure on the main bearing surface is N_1, the deformation Δ of the main bearing surface and the respective gaps Δx_2 and Δx_3 of the other two pairs of contact surfaces can be obtained. Therefore, when the fitting clearance between the main bearing surface is δ, the fitting clearance between the three pairs of contact surfaces of the fir-tree tenon joint structure can be expressed in the following equation:

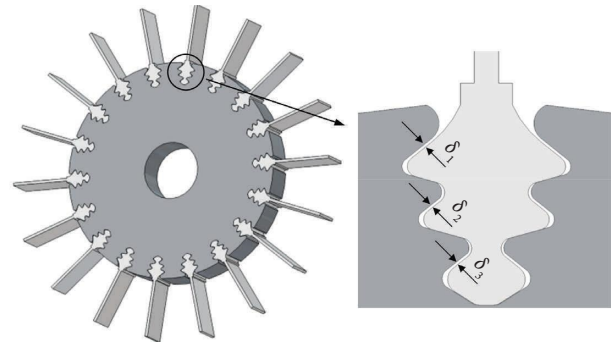

Figure 3: The fir-tree tenon connecting the blade and blade disc.

$$\begin{cases} \delta_1 = \delta, \\ \delta_2 = \delta + \Delta_2, \\ \delta_3 = \delta + \Delta_3. \end{cases} \tag{13}$$

4. Newmark-β Numerical Integration Method and Model Validation

4.1. Newmark-β Numerical Integration Method. Newmark-β numerical integration method is a common method for solving differential equations. Since the Newmark-β numerical integration method has the advantages of high accuracy, fast calculation, and high stability, it is widely used in the numerical calculation of the dynamic response of structures. In order to obtain the nonlinear dynamic response of the fir-tree tenon blade, the Newmark-β numerical integration method is used to solve the dynamic equation of the blade in this paper.

According to the abovementioned, the dynamic equation of the fir-tree tenon blade is as follows:

$$\mathbf{M}\ddot{\mathbf{X}} + \mathbf{C}\dot{\mathbf{X}} + \mathbf{K}\mathbf{X} = \mathbf{Q} - \mathbf{F}. \tag{14}$$

It is assumed that the displacement and velocity of the blade at the moment t_i are $\mathbf{X}_i$ and $\dot{\mathbf{X}}_i$. According to the blade dynamics equation, the acceleration of the blade is as follows:

$$\ddot{\mathbf{X}}_i = \mathbf{M}^{-1}\left(\mathbf{Q}_i - \mathbf{F}_i - \mathbf{C}\dot{\mathbf{X}}_i - \mathbf{K}\mathbf{X}_i\right). \tag{15}$$

According to the displacement $\mathbf{X}_i$, velocity $\dot{\mathbf{X}}_i$, and acceleration $\ddot{\mathbf{X}}_i$ of the blade at the moment t_i, the vibration displacement $\mathbf{X}_{i+1}$ of the blade at the moment t_{i+1} can be obtained as follows:

$$\mathbf{X}_{i+1} = \hat{\mathbf{K}}^{-1}\hat{\mathbf{Q}}_{i+1}, \tag{16}$$

where

$$\begin{cases} \hat{\mathbf{K}} = \mathbf{K} + \dfrac{1}{\beta\Delta t^2}\mathbf{M} + \dfrac{\alpha}{\beta\Delta t}\mathbf{C}, \\ \hat{\mathbf{Q}}_{i+1} = \mathbf{Q}_{i+1} - \mathbf{F}_{i+1} + \left[\dfrac{1}{\beta\Delta t^2}\mathbf{X}_i + \dfrac{1}{\beta\Delta t}\dot{\mathbf{X}}_i + \left(\dfrac{1}{2\beta} - 1\right)\ddot{\mathbf{X}}_i\right]\mathbf{M} \\ \quad + \left[\dfrac{\alpha}{\beta\Delta t}\mathbf{X}_i + \left(\dfrac{\alpha}{\beta} - 1\right)\dot{\mathbf{X}}_i + \dfrac{\Delta t}{2}\left(\dfrac{\alpha}{\beta} - 2\right)\ddot{\mathbf{X}}_i\right]\mathbf{C}. \end{cases} \tag{17}$$

It is assumed that the acceleration of the blade changes linearly in $\Delta t = t_{i+1} - t_i$. The acceleration $\ddot{\mathbf{X}}_{i+1}$ and velocity $\dot{\mathbf{X}}_{i+1}$ of the blade at the moment t_{i+1} can be expressed as follows:

$$\begin{cases} \ddot{\mathbf{X}}_{i+1} = \dfrac{1}{\beta\Delta t^2}\left(\mathbf{X}_{i+1} - \mathbf{X}_i\right) - \dfrac{1}{\beta\Delta t}\dot{\mathbf{X}}_i - \left(\dfrac{1}{2\beta} - 1\right)\ddot{\mathbf{X}}_i \\ \dot{\mathbf{X}}_{i+1} = \dfrac{\alpha}{\beta\Delta t}\left(\mathbf{X}_{i+1} - \mathbf{X}_i\right) + \left(1 - \dfrac{\alpha}{\beta}\right)\dot{\mathbf{X}}_i + \left(1 - \dfrac{\alpha}{2\beta}\right)\ddot{\mathbf{X}}_i\Delta t, \end{cases} \tag{18}$$

where the values of parameters α and β are 0.5 and 0.25. The Newmark-β numerical integration method is unconditionally stable under this condition.

4.2. Model Validation. In order to verify the correctness of the dry friction model and the blade dynamics model developed in this paper, the results of the amplitude-frequency curves are compared with those of [6]. As the blade in the reference is a dovetail blade, the forces applied to the dovetail tenon root in the reference are all applied to the 3rd pair of contact surfaces of the fir-tree tenon root in this paper to simulate the forces applied to the dovetail tenon root in the reference. Secondly, the geometric and material parameters of the blade in this paper are adjusted to match those of the blade in the reference, and exactly the same external excitation $Q = 500\sin(\omega t)$ is applied at the same location as the reference blade. Finally, taking the blade speed of 200 rad/s and 300 rad/s, respectively, the amplitude-frequency curve of the blade is made and compared with the reference. The specific implementation scheme of the finite element model verification is shown in Figure 4, and the comparison results are shown in Figure 5.

In Figure 5, the solid and dashed lines show the amplitude-frequency curves of the dovetail blade in the reference at 200 rad/s and 300 rad/s, respectively, while the dots and stars show the amplitude-frequency curves of the blade in this paper at 200 rad/s and 300 rad/s, respectively. As can be seen from the data in the graph, when the speed is 200 rad/s, the absolute error in amplitude is the greatest at $\omega = 1740$ with a value of -2.92×10^{-5} mm, and the relative error is the greatest at $\omega = 220$ with a value of 2.55%. When the rotation speed is 300 rad/s, the absolute error in amplitude is the greatest at $\omega = 1630$ with a value of 2.64×10^{-5} mm, and the relative error is the greatest at $\omega = 200$ with a value of 2.20%. As both the absolute and relative errors are small and within allowable limits, the dry friction model and kinetic model developed in this paper can be proved to be correct.

5. Results and Discussion

In order to further explore the vibration characteristics of the fir-tree tenon blade, this section analyzes the forced vibration response of the blade under different pressure distributions, tenon angle, friction coefficient, rotation speed, and aerodynamic excitation. Firstly, the geometrical and material parameters of the blade system are determined and the specific values are shown in Table 3. Secondly, it is assumed that the friction coefficient on each contact surface of the tenon and tenon groove is the same, and the shear stiffness of the three pairs of contact surfaces is $k_{ij} = 8 \times 10^6$ N/m. Finally, the harmonic excitation $P(t) = A\sin(\omega t + \varphi)$ acting on the middle of the blade is used to simulate the external excitation of the blade, where the excitation amplitude $A = 500$ N, and ω and φ represent the excitation angular frequency and phase, respectively.

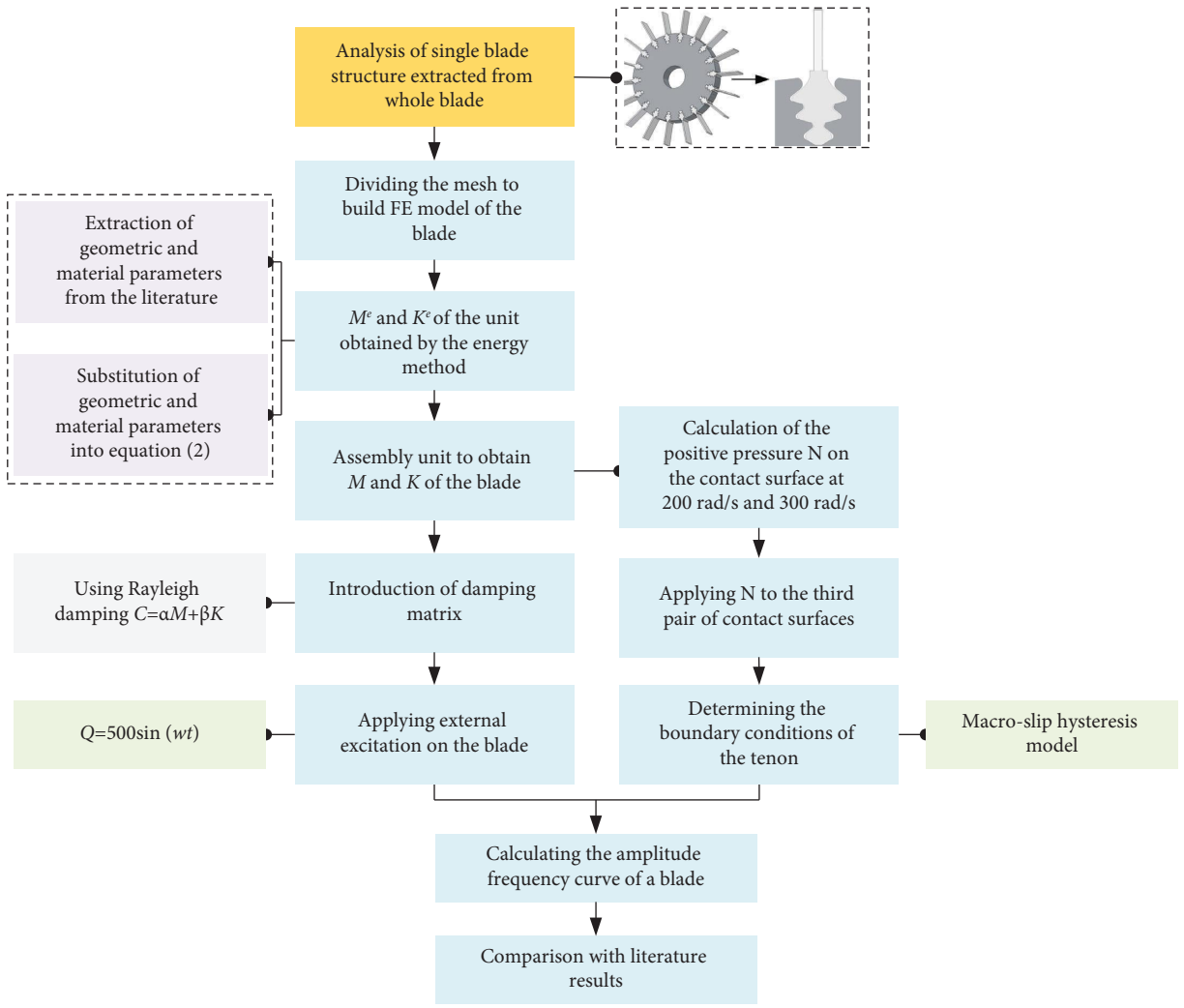

Figure 4: The specific implementation scheme of finite element model verification.

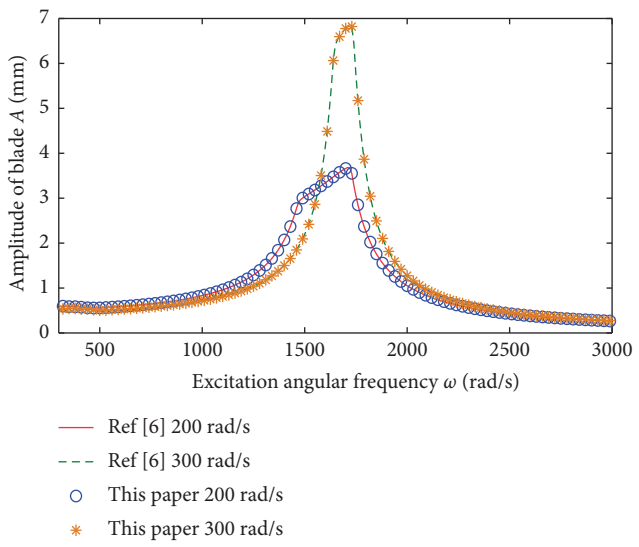

Figure 5: The model verification of the amplitude-frequency curve.

Table 3: The values of blade system parameters.

Symbols	Value	Unit
R	350	mm
L	150	mm
B	60	mm
H	7	mm
N	100	—
E	200	Pa
υ	0.3	—
ρ	7850	kg/m^3
κ	1.2	—

5.1. The Influence of Pressure Distribution. It is known that different contact modes of the fir-tree tenon will lead to significant changes in nonlinear forced response. Considering that different fitting clearances will greatly change the distribution mode of pressure on the root of the fir-tree blade, so as to change the boundary conditions of the blade, and then affect the vibration characteristics of the blade. In

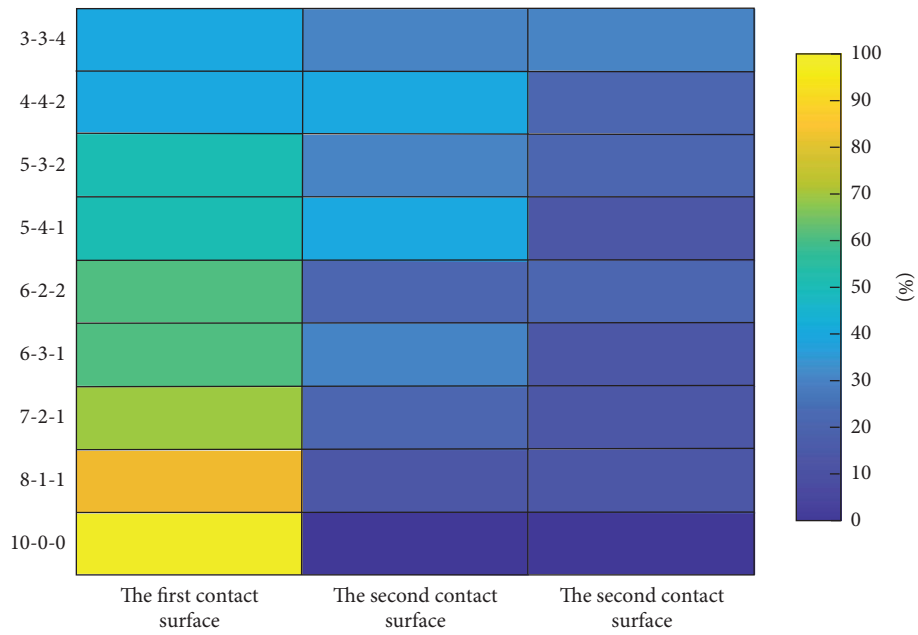

Figure 6: Pressure distribution cloud diagram of fir-tree tenon structure.

order to intuitively show the pressure distribution mode of the fir-tree tenon structure, the pressure distribution cloud diagram of the fir-tree tenon structure is made. The results are shown in Figure 6.

In order to further study the influence law of pressure distribution on blade vibration characteristics, the friction coefficient of the blade tenon root contact surface is 0.1. The amplitude-frequency response curves of the blade tip under different pressure distributions are made to observe the influence of pressure distribution, and the results are shown in Figures 7 and 8. As can be seen from the figure, both the positions of the main bearing surface and the pressure distribution have a significant influence on the vibration characteristics of the blade. When the rotational speed is low, the fir-tree tenon joint structure has a better vibration reduction effect in the case of only one pair of contact surfaces acting than in the case of three pairs of contact surfaces acting together, and the peak clipping phenomenon of the amplitude-frequency curve is more obvious when a pair of contact surfaces acting. When a pair of contact surfaces acts, the position of the bearing surface does not affect the vibration characteristics of the blade. When the three pairs of contact surfaces work together, the first pair of contact surfaces as the main bearing surface will make the tenon structure have a better damping effect. With the increase in speed, when a pair of contact surfaces of the tenon joint structure is used, the vibration reduction effect of the tenon joint structure is the worst, and the peak clipping phenomenon of the blade amplitude-frequency curve almost disappears, which is due to the fact that when the pressure is applied to a pair of contact surfaces, the pressure on a single contact surface is too large, resulting in the sticking between the tenon root and the tenon groove more easily, thus losing the original vibration reduction effect. Under the joint action of three pairs of contact surfaces of the tenon joint structure, the first pair of contact surfaces as the main bearing surface will make the tenon structure have a better vibration reduction effect, and the greater the pressure of the main bearing surface, the better the vibration reduction effect of the tenon joint structure, and the peak clipping phenomenon of the amplitude-frequency curve is more obvious. The resonance frequency of the blade under three pairs of contact surfaces is larger than that under a single contact surface. When the rotational speed is high, the vibration reduction effect of the tenon joint structure with three pairs of contact surfaces is still better than that of the tenon joint structure with a single pair of contact surfaces, and the resonance frequency of the blade is higher. However, in the case of the tenon joint structure with three pairs of contact surfaces, the position of the main bearing surface and the pressure distribution between the three pairs of contact surfaces have almost no influence on the vibration characteristics of the blade. Therefore, when the pressures on the three pairs of contact surfaces are the same, not only is the vibration amplitude of the blade lower, but the stresses in the tenon joint structure are also minimal.

Because the tenon structure relies on friction energy consumption to reduce the vibration amplitude of the blade, the magnitude of friction energy consumption directly reflects the damping effect of the tenon structure. When the rotational speed is 300 rad/s, the hysteresis curves on the contact surface of the tenon under different pressure distributions are made. The results are shown in Figure 9. It can be seen from the figure that the area enclosed by the hysteresis curve is the energy consumed by friction. When the rotational speed is low, the total friction force of the contact surface under the two pressure distribution modes is the same, but the tenon displacement of the single-contact surface is greater than that of the three contact surfaces. Therefore, the tenon structure with single contact surface

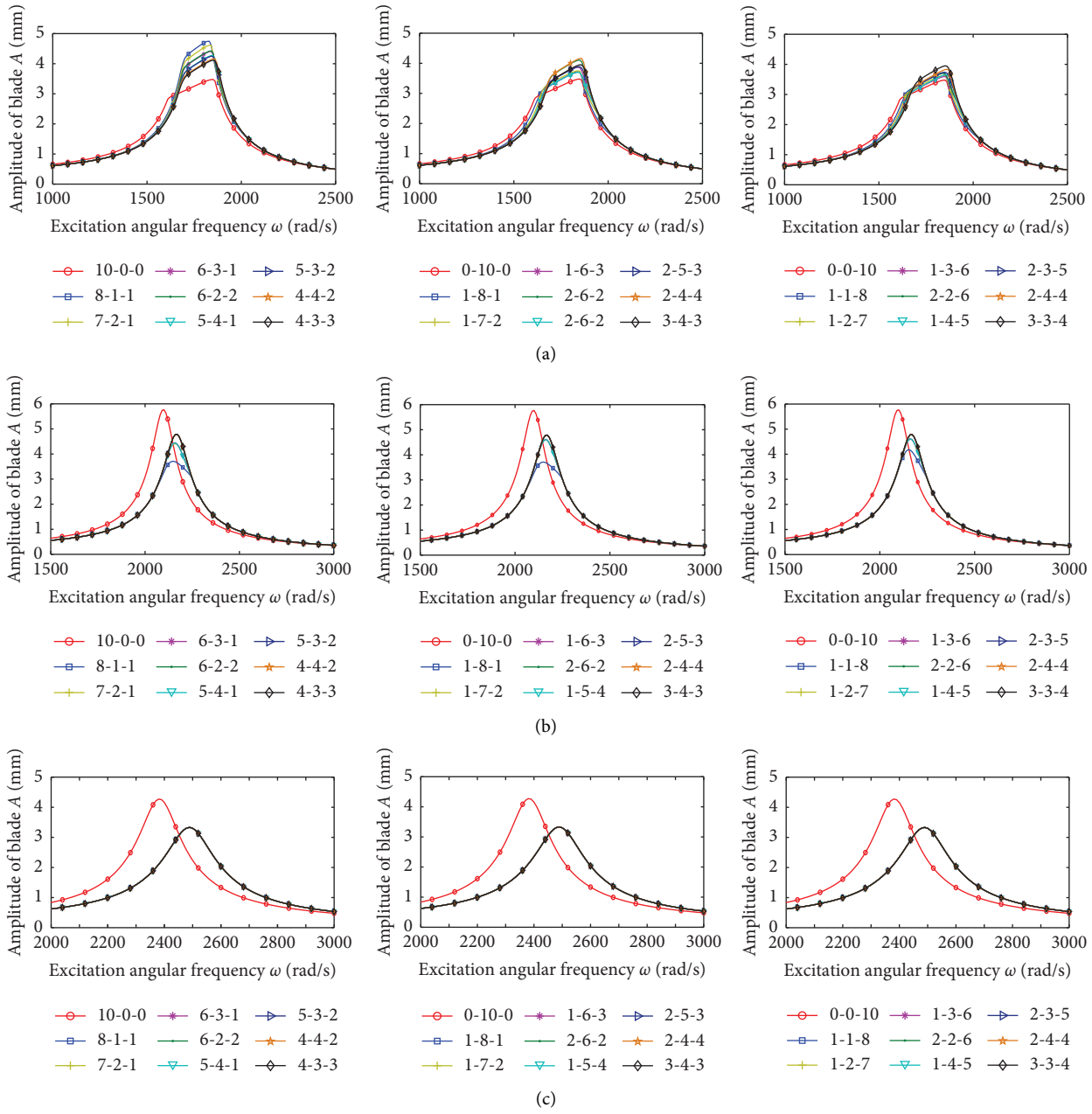

FIGURE 7: The amplitude-frequency curves of the blade at different pressure distributions for speeds of: (a) 300 rad/s, (b) 600 rad/s and (c) 800 rad/s.

consumes more energy, and the vibration amplitude of the blade is smaller. However, with the increase of rotational speed, the positive pressure of the contact surface of the tenon is too large when the single-pair contact surface acts, which makes the contact surface more prone to stick. However, with the increase of rotational speed, the positive pressure of the contact surface of the tenon is too large when the single contact surface acts, which makes the contact surface more prone to stick. Therefore, the vibration reduction effect of the tenon structure with the single-contact surface is much worse than that of the tenon structure with multiple contact surfaces.

In summary, the fir-tree tenon joint structure can exert better vibration reduction performance only at higher speeds. When the first pair of the contact surface is the main bearing surface, the vibration reduction effect of the fir-tree tenon joint structure is the best, and the higher the contact pressure of the main bearing surface, the better the vibration reduction effect of the tenon structure. Therefore, under the premise of ensuring strength, the main bearing surface should be subjected to a greater proportion of pressure as far as possible. When the rotational speed is further improved, the average force of the three pairs of contact surfaces of the tenon structure can not only have the best damping effect but also bear the minimum stress.

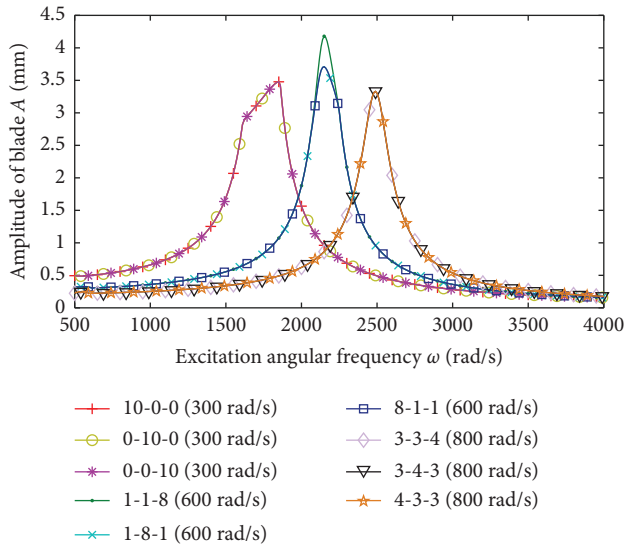

Figure 8: The amplitude-frequency curve of the blade at the pressure distribution with the best vibration reduction effect at each speed.

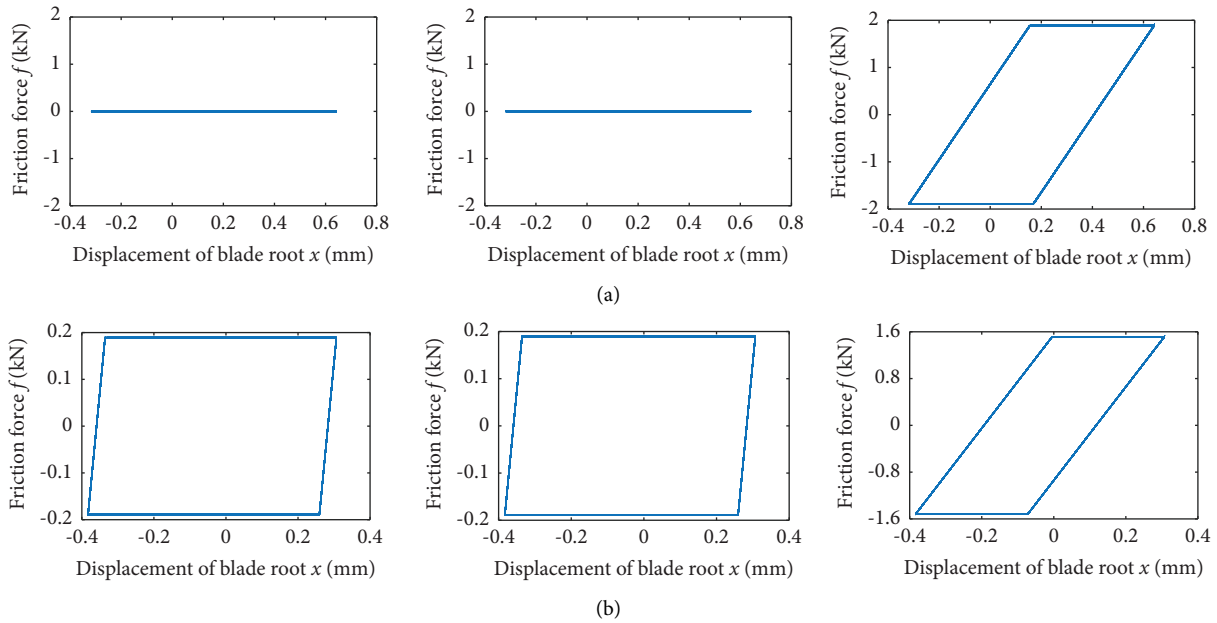

Figure 9: The hysteresis curves on the contact surface of the tenon joint structure at different pressure distributions at 300 rad/s: (a) under 0-0-10 pressure distribution and (b) under 1-1-8 pressure distribution.

5.2. The Influence of Tenon Angle. The tenon angle is one of the main parameters of the tenon structure. According to the principle of force balance, it can be seen that the change of tenon angle directly affects the normal pressure on the contact surface, but at the same time, it also affects the friction force on the contact surface in the direction of blade vibration. In order to investigate the influence of tenon angle variation on the vibration characteristics of rotating blades, the relationship between tenon angle and normal pressure on the contact surface and the relationship between tenon angle and dry friction is derived from theory.

When the blade is rotating, the vibration displacement $\mathbf{y}(t)$ in the transverse direction of the blade should satisfy the kinetic equation (14).

$$\mathbf{M}\ddot{\mathbf{y}} + \mathbf{C}\dot{\mathbf{y}} + \mathbf{K}\mathbf{y} = \mathbf{F}(t) - \mathbf{f}_n, \tag{19}$$

when the tenon angle changes, the blade mass $\mathbf{M}$, the stiffness $\mathbf{K}$, the damping matrix $\mathbf{C}$, and the external excitation $\mathbf{F}(t)$ do not change as the blade speed and external excitation remain unchanged.

It is assumed that the components of the positive pressure of the three pairs of contact surfaces in the y-direction are N_1, N_2, and N_3, respectively. Taking the first pair of contact surfaces as an example, according to the balance principle of force and the geometric relationship of structure, the positive pressure N_{11} and N_{12} of the contact surface can be expressed by equation (15).

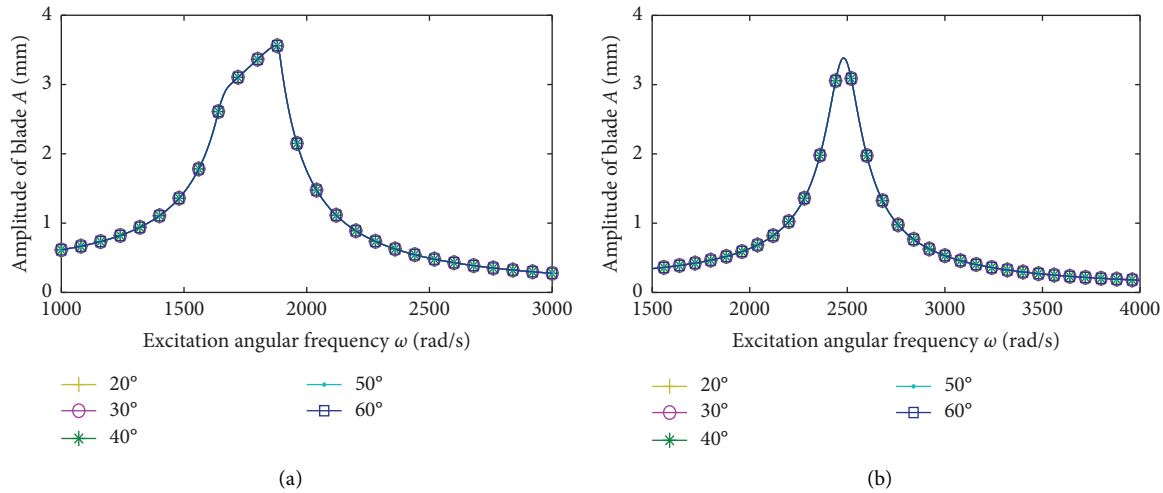

Figure 10: The amplitude-frequency curve of the blade at different tenon angles: (a) at 300 rad/s and (b) at 800 rad/s.

$$N_{11} = \frac{\sin\beta_1}{\sin(\alpha_1+\beta_1)}N_1,$$
$$N_{12} = \frac{\sin\alpha_1}{\sin(\alpha_1+\beta_1)}N_1. \tag{20}$$

By projecting the friction f_{11} and f_{12} on the contact surfaces of the tenon in the y-direction, the component f_1 of the dry friction in the y-direction can be obtained. f_1 can be represented by equation (16).

$$\begin{aligned} f_1 &= f_{11}\sin\alpha_1 + f_{12}\sin\beta_1 \\ &= \mu N_{11}\sin\alpha_1 + \mu N_{12}\sin\beta_1 \\ &= \mu N_1\frac{\cos\beta_1\sin\alpha_1}{\sin(\alpha_1+\beta_1)} + \mu N_1\frac{\cos\alpha_1\sin\beta_1}{\sin(\alpha_1+\beta_1)}. \end{aligned} \tag{21}$$

In order to balance the component of the positive pressure on the contact surface in the x-direction, it is necessary to make the tenon angle $\alpha_1 = \beta_2 = \eta$. The equation (21) can be expressed as follows:

$$\begin{aligned} f_1 &= \mu N_1\frac{\sin\eta\cos\eta}{\sin(2\gamma)} + \mu N_1\frac{\sin\eta\cos\eta}{\sin(2\gamma)} \\ &= \mu N_1\frac{\sin\eta\cos\eta}{2\sin\eta\cos\eta} + \mu N_1\frac{\sin\eta\cos\eta}{2\sin\eta\cos\eta} \\ &= \mu N_1. \end{aligned} \tag{22}$$

It can be found that when the tenon angles α_1 and β_2 are changed at the same time, the friction force of the contact surface in the y-direction is not affected. The change of the tenon angle will not affect the vibration differential equation of the blade, so changing the tenon angle of the tenon structure does not affect the response results of the blade. However, the change of tenon angles α_1 and β_2 will directly affect the positive pressure of the contact surface, thus affecting the service life of the blade.

When the rotational speed is 300 rad/s and 800 rad/s, the amplitude-frequency curve of the blade is shown in Figure 10 under different tenon angles. It can be found that the change of the tenon angle does not affect the amplitude of the blade, and the result is also consistent with the previous prediction. When the tenon angle is $\alpha_1 = \beta_1 = \eta$, according to equation (15), the positive pressure of the contact surface is as follows:

$$N_{11} = N_{12} = \frac{1}{2\cos\eta}N_1. \tag{23}$$

According to equation (23), it can be found that as the tenon angle increases, the contact pressure will gradually increase. On the premise of ensuring the effective joint of the tenon structure, reducing the tenon angle as much as possible can improve the service life of the blade.

5.3. The Influence of Friction Coefficient. The vibration amplitude of the blade can be reduced by the friction energy dissipation of the tenon structure. The change of friction coefficient will directly affect the size of dry friction, thus affecting the vibration characteristics of the blade. Therefore, it is necessary to study the influence of friction coefficient on blade vibration. The blade speed is controlled at 200 rad/s and 300 rad/s, respectively, and the amplitude-frequency curves of the blade under different friction coefficients are made to analyze the influence of friction coefficient on the vibration reduction characteristics of the blade. The results are shown in Figure 11. It can be seen from the figure that the friction coefficient of the tenon contact surface has a very significant indigenous influence on the vibration characteristics of the blade. When the rotational speed is constant, the resonance amplitude of the blade increases with the increase of the friction coefficient of the tenon contact surface and the resonance frequency of the blade decreases. When the friction coefficient is small, the peak clipping phenomenon of the response can be obviously observed in the amplitude-frequency curve of the blade, but with the

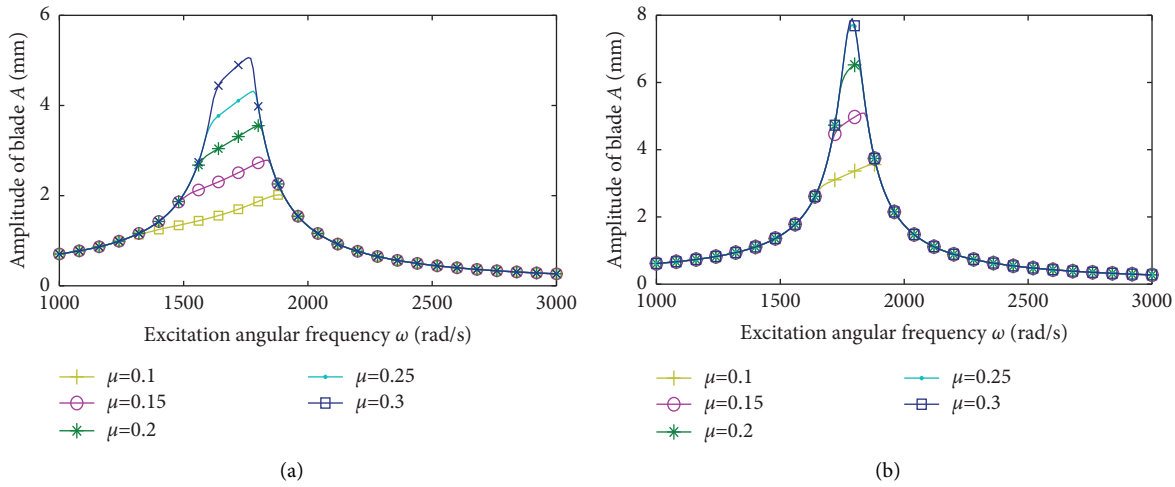

Figure 11: The amplitude-frequency curve of the blade under different friction coefficients: (a) at 200 rad/s and (b) at 300 rad/s.

increase of the friction coefficient, the peak clipping phenomenon will become weaker and weaker until it disappears. The reason for this phenomenon is that when the friction coefficient is small, the contact surface between the tenon and the tenon groove slips due to the small critical friction force, resulting in the peak clipping phenomenon in the amplitude-frequency curve. However, with the increase of friction coefficient, the critical friction force is also increasing, which makes the sliding between the tenon and the tenon groove more and more difficult. When the contact surface between the tenon and the tenon groove is viscous, the peak clipping phenomenon in the amplitude-frequency curve of the blade disappears. In the case of the same friction coefficient, the increase of rotational speed will increase the resonant amplitude of the blade and weaken the peak clipping phenomenon. Therefore, the tenon joint structure will play a better vibration reduction effect when the friction coefficient is low.

In order to further study the influence of friction coefficient on the vibration reduction performance of the tenon joint structure, the excitation frequency is 1800 Hz near the first natural frequency of the blade, and the blade speed is 300 rad/s. The time domain response diagram, frequency spectrum diagram, and the hysteresis curve of dry friction with the displacement of the blade root with a friction coefficient of 0.1, 0.2, and 0.3 are respectively made. The results are shown in Figure 12. It can be seen from the figure that the larger the friction coefficient is, the smaller the displacement amplitude of the blade root is. Moreover, when the friction coefficients are 0.1 and 0.2, there are obvious harmonic phenomena in the time domain diagram of the blade root. At the same time, in the frequency domain diagram of the blade root, in addition to the main frequency, there are obvious triple and quintuple frequencies. However, when the friction coefficient is 0.3, the harmonic phenomenon of the blade root disappears, and the displacement of the blade root shows a strict harmonic change over time. At the same time, there is only a principal frequency component in the frequency domain diagram, and there is no obvious triple and quintuple frequency. The dry friction of the tenon root increases with the increase of friction coefficient, but the slip distance of the contact surface decreases with the increase of friction coefficient. When the friction coefficients are 0.1 and 0.2, the dry friction and displacement show a piecewise linear overall nonlinear relationship, but when the friction coefficient is 0.3, the dry friction and displacement show a strictly linear relationship. Finally, the energy consumed by the dry friction decreases with the increase of the friction coefficient, and when the friction coefficient is 0.3, the dry friction no longer does the power consumption energy. From the abovementioned analysis, it can be found that the friction energy is the cause of the hard nonlinearity of the blade amplitude-frequency curve, and it is also the cause of the harmonic phenomenon in the blade root time domain diagram and the triple frequency and five times frequency in the spectrum diagram. It is because the energy dissipation of dry friction decreases with the increase of friction coefficient, which leads to the increase of the resonant amplitude with the increase of friction coefficient.

In summary, the increase of the friction coefficient will weaken the vibration reduction performance of the fir-tree tenon structure, making the blade more prone to fatigue damage, but the increase of friction coefficient has little effect on the contact pressure. Therefore, the stability and service life of the blade can be improved by minimizing the roughness of the contact surface under economic conditions.

5.4. The Influence of Rotational Speed. The rotational speed of the blade directly affects the size of the centrifugal force and thus changes the dry friction of the tenon root. Due to the centrifugal stiffening effect of the blade, the increase of rotational speed will change the stiffness of the blade. Therefore, it is necessary to study the vibration characteristics of blades at different speeds. Taking the friction coefficient of the tenon root contact surface of the blade as 0.1, the amplitude-frequency response curve of the blade under

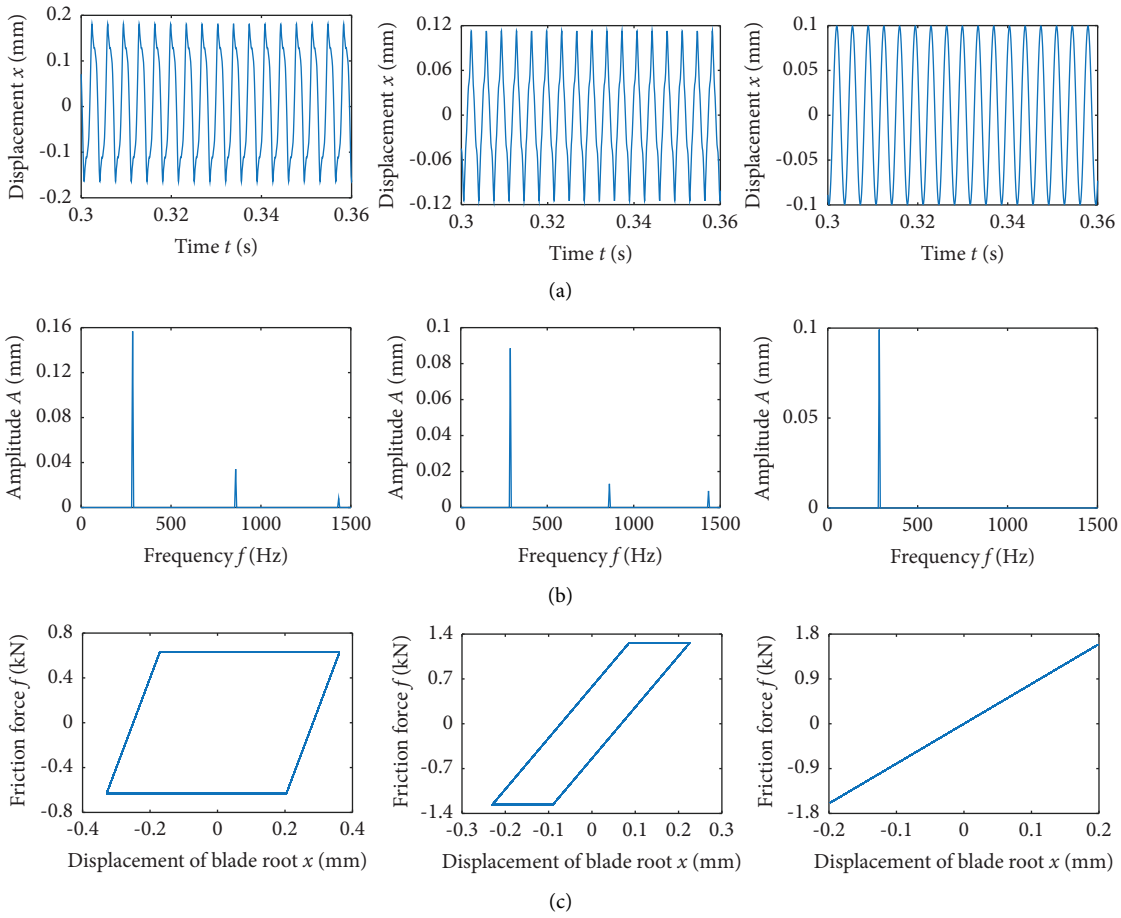

Figure 12: The response curves of the blade root at different friction coefficients: (a) the time domain response diagram, (b) the frequency spectrum diagram, and (c) the hysteresis curve.

different rotational speeds is made to observe the influence of rotational speed. The results are shown in Figure 13. It can be seen from the figure that when the blade speed is not high, the amplitude-frequency response curve of the blade shows a certain peak clipping phenomenon. The resonance frequency of the blade increases with the increase of rotational speed, and the resonance peak increases with the increase of rotational speed, and the resonance peak is significantly lower than that without a peak clipping phenomenon. When the rotational speed of the blade is not less than 600 rad/s, there is no obvious peak clipping phenomenon in the amplitude-frequency response curve of the blade at this time. However, with the increase of the rotational speed, the resonant frequency of the blade gradually increases, and the resonant peak gradually decreases. It can also be seen from the figure that when the blade speed is low, the blade exhibits a certain soft nonlinear phenomenon at a low frequency, and the blade amplitude is larger than that at a high frequency.

In order to further study the influence of rotational speed on the vibration characteristics of the blade, the excitation frequency is taken as the frequency near the first-order natural frequency of the blade, and the time domain response diagram, frequency spectrum diagram, and the hysteresis curve of dry friction with displacement change at

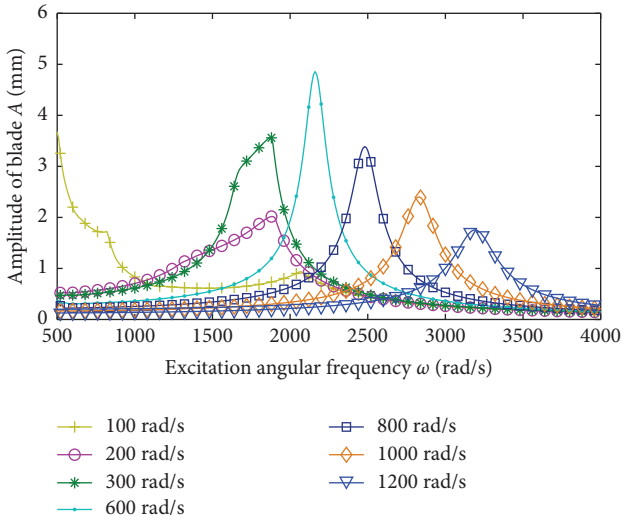

Figure 13: The amplitude-frequency curve of the blade at different rotational speeds.

rotational speeds of 200 rad/s, 300 rad/s, and 600 rad/s are respectively made. The results are shown in Figure 14. It can be seen from the figure that the larger the rotational speed is,

the smaller the displacement amplitude of the blade root is. When the rotational speed is 200 rad/s and 300 rad/s, the nonlinear dry friction at the blade root causes an obvious harmonic phenomenon in the time domain diagram. At the same time, in the blade root frequency domain diagram, there are three and five frequencies in addition to the main frequency. However, when the rotational speed is 600 rad/s, the dry friction of the blade root changes linearly with the displacement, the time domain diagram of the blade root is harmonic, and the response amplitude is greatly reduced. At the same time, there is only the main frequency component in the frequency domain diagram. Secondly, the dry friction of the tenon root increases with the increase of rotational speed, but the slip distance between the contact surfaces of the tenon joint structure decreases with the increase of rotational speed. Finally, the energy consumed by the dry friction increases first. It then decreases with the increase of the rotational speed, and when the rotational speed is 600 rad/s, the dry friction no longer does the power consumption energy. From the abovementioned analysis, it can be found that for the blade with the same parameters, when the rotational speed increases, the resonant amplitude value of the blade first increases and then decreases. The reason for the increase is that the increase of the blade energy plays a major role, and the reason for the decrease is that the centrifugal stiffening effect of the blade plays a major role. Nonlinear phenomena become weaker and weaker with the increase of rotational speed until they disappear. The vibration reduction effect of the tenon structure increases first and then decreases with the increase of rotational speed. There is an optimal rotational speed for the blade with specific parameters, which makes the tenon structure have the best vibration reduction effect, and the blade amplitude decreases the most.

The blade rotation speed has a great influence on the positive pressure of the contact surface. According to the equations (8)–(10), it can be seen that the positive pressure of the contact surface of the tenon root is directly related to the centrifugal force of the blade, and the centrifugal force of the blade is proportional to the square of the rotational speed. Therefore, with the increase of the rotational speed of the blade, the contact pressure of the tenon root will increase significantly.

In summary, the increase of rotational speed will make the forced response of the blade increase first and then decrease, while the contact pressure will gradually increase. Therefore, at low rotational speed, the forced response of the blade and the stress of the tenon structure are small, and the blade is not prone to fatigue failure. There is an optimal rotational speed that makes the tenon structure have the best vibration reduction effect.

5.5. The Influence of Aerodynamic Excitation. The blade in the process of working due to the engine structure will be subject to the action of aerodynamic excitation. In order to study the vibration characteristics of the blade under aerodynamic excitation, the number of stator blades in front of rotor blades is $N = 5$. When the rotating speed of the blade is Ω, the aerodynamic excitation $Q(t)$ can be expressed as follows:

$$Q(t) = A_0 \sin(N\Omega t), \tag{24}$$

where A_0 is the aerodynamic excitation amplitude.

Because the aerodynamic excitation amplitudes of different engines such as aeroengine and ground gas turbine and different positions of the same engine are quite different, it is necessary to study the vibration characteristics of blades under different excitation amplitudes. The amplitude-frequency response curves of the blade under different aerodynamic excitation amplitudes are made, and the results are shown in Figure 15. It can be seen from the figure that when the amplitude of the aerodynamic excitation is not high, the vibration peak of the blade is low, and the amplitude-frequency response curve does not appear peak clipping phenomenon. With the increase of aerodynamic excitation amplitude, the resonance frequency and resonance peak of the blade increase, and the nonlinear region of the amplitude-frequency response curve becomes wider and the peak clipping phenomenon becomes more obvious. The reason for this phenomenon is that as the excitation amplitude increases, the vibration amplitude of the blade also increases, resulting in an increase in the slip distance of the tenon root and an increase in friction energy consumption. At the same time, the increase of excitation amplitude increases the rotational speed when the tenon root is viscous, which increases the resonance frequency of the blade and makes the peak clipping phenomenon more obvious. However, when the aerodynamic excitation amplitude is greater than 400 N and the speed is between 350 rad/s and 400 rad/s, the vibration amplitude of the blade is almost unchanged with the increase of the aerodynamic excitation amplitude. From an energy point of view, it can be seen that the fir-tree tenon structure has good vibration reduction ability, which can resist the influence of aerodynamic excitation amplitude and stabilize the vibration amplitude of the blade in a certain range. When the excitation amplitude is constant, the response amplitude of the blade increases first and then decreases with the increase of the rotational speed, which is the same as the changing trend of the blade amplitude with the rotational speed under harmonic excitation. It proves the correctness of using harmonic excitation to analyze blade vibration characteristics.

In summary, the increase of the aerodynamic excitation amplitude will cause the blade resonance peak to increase, making the nonlinear region of the amplitude-frequency response curve wider and the peak clipping phenomenon more obvious. When the speed is between 350 rad/s and 400 rad/s, the vibration amplitude of the blade is the least affected by the aerodynamic excitation. Although the excitation amplitude increased significantly, the amplitude of the blade can be stabilized in a certain range. Using intermittent excitation to simulate the force of the blade can not only correctly analyze the nonlinear vibration response of the blade, but also make the excitation frequency and the blade rotation speed independent of each other. In this way, the vibration characteristics of blades at different speeds can be analyzed more comprehensively, which has a better guiding value for the general design of blades.

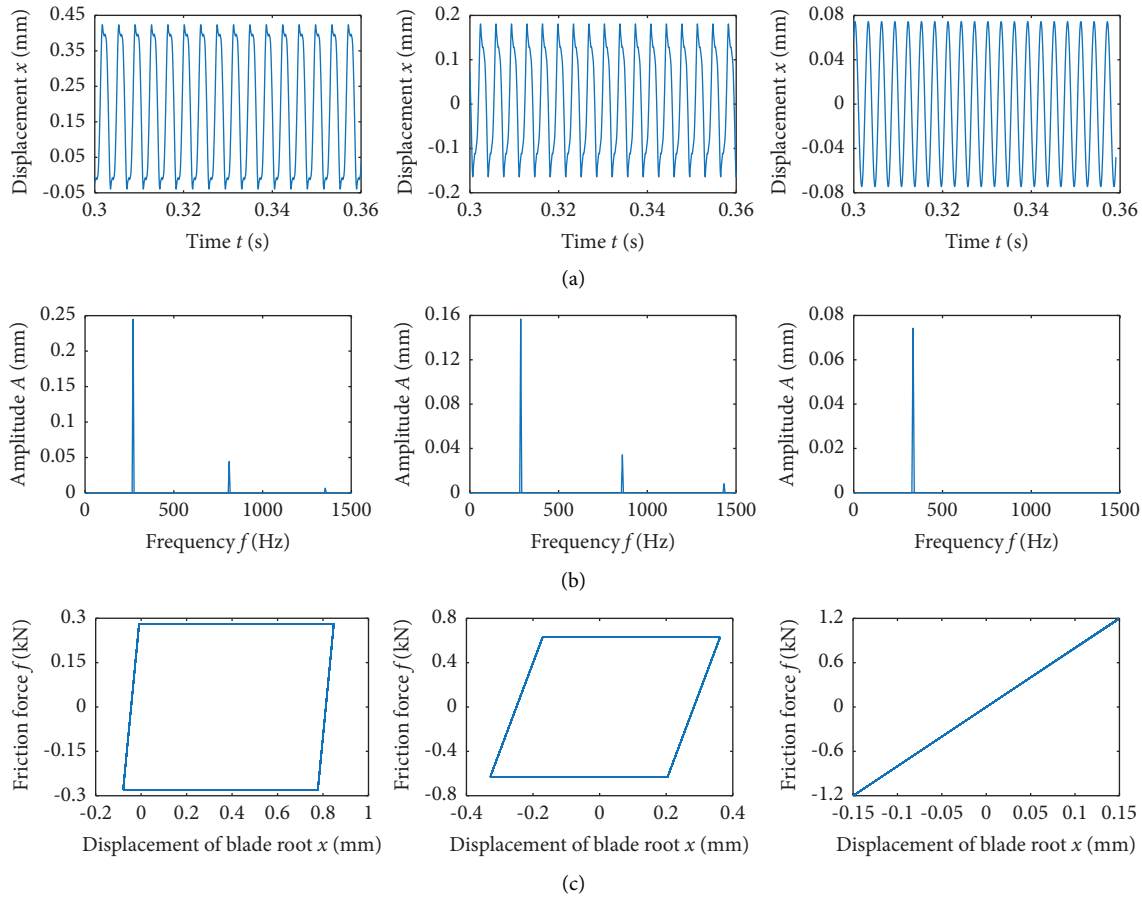

Figure 14: The response curves of the blade root at 200 rad/s, 300 rad/s, and 600 rad/s speeds: (a) the time domain response diagram, (b) the frequency spectrum diagram., and (c) the hysteresis curve.

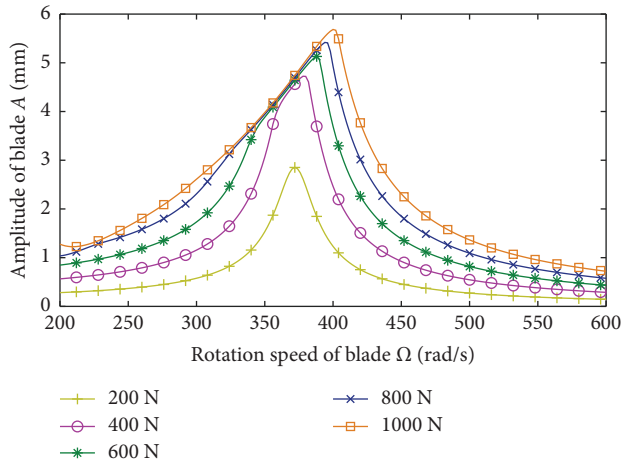

Figure 15: The amplitude-frequency curve of the blade at different aerodynamic excitation amplitudes.

6. Conclusion

In this paper, the fir-tree tenon blade is taken as the research object. After the blade is discretized by the finite element method, the dynamic model of the rotating blade is established by using the elastic structure analysis theory, the minimum potential energy principle, and numerical integration. According to the ideal dry friction theory, a dry friction model is established to simulate the nonlinear friction of the tenon joint structure, so as to determine the boundary conditions of the blade. The Newmark method is used to solve the dynamic equation of the blade. The influence of pressure distribution, tenon angle, friction coefficient, blade rotation speed, and aerodynamic excitation on blade vibration characteristics is analyzed and the following conclusions are obtained:

(1) The position of the main bearing surface of the tenon structure has a great influence on the vibration characteristics of the blade. In the case of the same rotational speed, whether it is single-sided contact or multisided contact; when the first pair of contact surfaces is the main bearing surface, the vibration reduction effect of the tenon structure is the best and the vibration amplitude of the blade is the lowest.

(2) The contact mode and pressure ratio of the tenon structure have a great influence on the vibration characteristics of the blade. The damping effect of single-surface contact is better when the rotational speed is low. The damping effect of multisurface contact is better when the rotational speed is high,

and the pressure ratio of the main bearing surface should be increased. However, when the rotational speed is too high, the average distribution pressure can make the vibration amplitude of the blade the lowest and the contact stress minimum.

(3) The friction coefficient and blade rotation speed have a great influence on the vibration amplitude of the blade, while the change of the tenon angle will not directly affect the vibration amplitude of the blade. The contact pressure of the tenon root is greatly affected by the tenon angle and the blade rotation speed.

(4) The increase of aerodynamic excitation will lead to the increase of blade vibration amplitude and make the nonlinear region of the amplitude-frequency response curve wider. There is a certain range of rotational speed, which makes the blade least affected by aerodynamic excitation, and the vibration amplitude of the blade is stable in a certain range.

Nomenclature

HBM: Harmonic balance method
DLFT: Dynamic Lagrangian frequency-time
CB-CMS: Craig–Bampton component mode synthesis

Symbols

Ω: The rotational speed of the system
R: Blade disc radius
L: Length of the blade
b: Width of the blade
h: Height of the blade
n: Number of the blade division elements
$l = L/n$: Length of the element
P_i: Any point in the i-th element
x_i: Distance from P_i to the first node of the i-th element
E: Young's modulus of the blade
v: Poisson's ratio of the blade
I: Moment of inertia of the blade section
ρ: The density of the blade
κ: Shear correction factor
w: Lateral displacement due to blade deformation
F_c: The centrifugal force of the blade
F_y: Lateral component of centrifugal force
γ: Shear strain due to shear force
θ: The rotation angle of the blade section
φ: Neutral shaft angle
Q^e: The energy of the element
U_b^e: The strain energy caused by the bending deformation of the element
U_s^e: The strain energy caused by the shear deformation of the element
U_c^e: The centrifugal strain energy of the element
T_b^e: The kinetic energy caused by the bending deformation of the element
T_s^e: The kinetic energy caused by the shear deformation of the element
ω_b^e: The displacements caused by the bending deformation
ω_s^e: The displacements caused by the shear deformation
$\mathbf{k}_b^e$: Element bending stiffness matrix
$\mathbf{k}_s^e$: Element shear stiffness matrix
$\mathbf{k}_c^e$: Element centrifugal stiffness matrix
$\mathbf{m}_b^e$, $\mathbf{m}_s^e$: Element mass matrices
$\mathbf{M}$: Mass matrix of the blade system
$\mathbf{K}$: Stiffness matrix of the blade system
ω_1, ω_2: The first two inherent frequencies of the system
ξ_1, ξ_2: The modal damping ratios
$\mathbf{Q}$: The external excitation
$\mathbf{F}$: The damping force
N: Centrifugal force on the blade
N_{ij}: Positive pressure generated by N on the i-th pair of contact surfaces j
$y\ (t)$: Displacement of blade roots in the horizontal direction
d_{ij}: Displacement of x on the tangent of the i-th pair of contact surfaces j
α_i: The angle between the i-th pair of contact surfaces 1 and the horizontal direction
β_i: The angle between the i-th pair of contact surfaces 2 and the horizontal direction
A_{ij}: The surface area of the i-th pair of contact surfaces j
w_{ij}: Displacement of the friction dampers on the i-th pair of contact surfaces j
k_{ij}: Coefficient of shear stiffness on the i-th pair of contact surfaces j
μ_{ij}: Coefficient of friction on the i-th pair of contact surfaces j
f_{ij}: Friction on the i-th pair of contact surfaces j
Δ: Deformation of the main bearing surface
Δx_2: The gap between the second pair of contact surfaces
Δx_3: The gap between the third pair of contact surfaces
k: The contact stiffness of the tenon
δ_1, δ_2, δ_3: The fitting clearances between the tenon root and tenon groove
δ: The fitting clearance between the main bearing surface
ω, φ: The excitation angular frequency and phase.

Data Availability

All data generated or analyzed during this study are included within the article, but the processed data required to reproduce these findings cannot be shared at this time due to legal or ethical reasons.

Conflicts of Interest

The authors declare that they have no conflicts of interest.

Acknowledgments

This project was supported by the National Natural Science Foundation of China (no. 52075086) and the Fundamental Research Funds for the Central Universities (no. N2203021).

References

[1] Z. Mazur, A. Hernández-Rossette, and R. García-Illescas, "Investigation of the failure of the L-0 blades," *Engineering Failure Analysis*, vol. 13, no. 8, pp. 1338–1350, 2006.

[2] J. Kubiak Sz, G. Urquiza B, C. J. García, and E. F. Sierra, "Failure analysis of steam turbine last stage blade tenon and shroud," *Engineering Failure Analysis*, vol. 14, no. 8, pp. 1476–1487, 2007.

[3] M. D. Ulriksen, J. F. Skov, K. A. Dickow, P. H. Kirkegaard, and L. Damkilde, "Modal analysis for crack detection in small wind turbine blades," *Key Engineering Materials*, vol. 569-570, pp. 603–610, 2013.

[4] C. D. Qin, D. Desai, and S. Heyns, "High cycle fatigue life prediction of steam turbine blade during transient resonant conditions," in *Proceedings of the International Conference on Energy and Mechanical Engineering*, pp. 1054–1062, Hubei, China, October 2016.

[5] X. H. Liang, M. J. Zuo, and Z. P. Feng, "Dynamic modeling of gearbox faults: a review," *Mechanical Systems and Signal Processing*, vol. 98, pp. 852–876, 2018.

[6] K. Feng, J. C. Ji, Q. Ni, and M. Beer, "A review of vibration-based gear wear monitoring and prediction techniques," *Mechanical Systems and Signal Processing*, vol. 182, Article ID 109605, 2023.

[7] S. Zucca, C. M. Firrone, and M. M. Gola, "Numerical assessment of friction damping at turbine blade root joints by simultaneous calculation of the static and dynamic contact loads," *Nonlinear Dynamics*, vol. 67, no. 3, pp. 1943–1955, 2012.

[8] Z. L. Chen, C. F. Li, Z. Y. Yang, and H. She, "A new method of micro-slip contact normal pressure modeling and its application in the dynamic analysis of the dovetail–tenon–mortise jointed blades," *Mechanics Based Design of Structures and Machines*, 2022.

[9] C. F. Li, Z. C. Shen, Z. L. Chen, and H. She, "A study on the vibration dissipation mechanism of the rotating blade with dovetail joint," *Journal of Low Frequency Noise, Vibration and Active Control*, vol. 40, no. 3, pp. 1271–1292, 2021.

[10] C. F. Li, X. W. Liu, Q. S. Tang, and Z. Chen, "Modeling and nonlinear dynamics analysis of a rotating beam with dry friction support boundary conditions," *Journal of Sound and Vibration*, vol. 498, Article ID 115978, 2021.

[11] J. Chen, C. Zang, B. Zhou, and E. Petrov, "A study of friction microslip modeling for dynamic analysis of bladed discs with root joints," *Proceedings of the Institution of Mechanical Engineers-Part C: Journal of Mechanical Engineering Science*, vol. 233, no. 8, pp. 2599–2614, 2019.

[12] J. Wang, T. Yu, Y. H. Zhang, and Q. K. Han, "Vibration and friction damping analysis of blades with dovetail attachment," *Journal of The Chinese Society of Mechanical Engineers*, vol. 40, no. 2, pp. 179–189, 2019.

[13] H. X. She, C. F. Li, Q. S. Tang, and B. Wen, "Nonlinear vibration analysis of a rotating disk-beam system subjected to dry friction," *Shock and Vibration*, vol. 2020, no. 7, Article ID 7604174, 19 pages, 2020.

[14] H. Ma, D. Wang, X. Tai, and B. Wen, "Vibration response analysis of blade-disk dovetail structure under blade tip rubbing condition," *Journal of Vibration and Control*, vol. 23, no. 2, pp. 252–271, 2017.

[15] E. Lemoine, D. Nélias, F. Thouverez, and C. Vincent, "Influence of fretting wear on bladed disks dynamic analysis," *Tribology International*, vol. 145, Article ID 106148, 2020.

[16] K. Asai, S. Sakurai, T. Kudo, N. Ozawa, and T. Ikeda, "Evaluation of friction damping in dovetail root joints based on dissipation energy on contact surfaces," in *Proceedings of the Asme Turbo Expo: Power for Land, Sea, & Air*, Orlando, FL, USA, June 2009.

[17] M. Huls, L. P. Scheidt, and J. Wallaschek, "Influence of geometric design parameters onto vibratory response and high-cycle fatigue safety for turbine blades with friction damper," *Journal of Engineering for Gas Turbines & Power*, vol. 141, no. 4, Article ID 041022, 2019.

[18] C. F. Li, Z. C. Shen, B. F. Zhong, and B. Wen, "Study on the nonlinear characteristics of a rotating flexible blade with dovetail interface feature," *Shock and Vibration*, vol. 2018, Article ID 4923898, 13 pages, 2018.

[19] C. F. Li, Z. Y. Yang, Z. L. Chen, and T. Jia, "Blade reduced model considering local contact and analyzing blade vibration characteristics," *Journal of Sound and Vibration*, vol. 557, Article ID 117772, 2023.

[20] E. P. Petrov and D. J. Ewins, "Effects of damping and varying contact area at blade-disk joints in forced response analysis of bladed disk assemblies," *Journal of Turbomachinery*, vol. 128, no. 2, pp. 403–410, 2006.

[21] S. A. Meguid, P. S. Kanth, and A. Czekanski, "Finite element analysis of fir-tree region in turbine discs," *Finite Elements in Analysis and Design*, vol. 35, no. 4, pp. 305–317, 2000.

[22] M. Lavella and D. Botto, "Fretting wear characterization by point contact of nickel superalloy interfaces," *Wear*, vol. 271, no. 9-10, pp. 1543–1551, 2011.

[23] A. Koscso and E. P. Petrov, "Blade root joint modelling and analysis of effects of their geometry variability on the nonlinear forced response of tuned and mistuned bladed disks," in *Proceedings of the ASME Turbo Expo 2020: Turbomachinery Technical Conference and Exposition*, Corners, Georgia, September 2020.

[24] E. Ferhatoglu and S. Zucca, "On the non-uniqueness of friction forces and the systematic computation of dynamic response boundaries for turbine bladed disks with contacts," *Mechanical Systems and Signal Processing*, vol. 160, Article ID 107917, 2021.

[25] W. Zhao, D. Zhang, and Y. H. Xie, "Vibration analysis of mistuned damped blades with nonlinear friction and contact," *Journal of Low Frequency Noise, Vibration and Active Control*, vol. 38, no. 3-4, pp. 1505–1521, 2019.

[26] A. Shukla and S. P. Harsha, "An experimental and FEM modal analysis of cracked and normal Steam Turbine Blade," *Materials Today: Proceedings*, vol. 2, no. 4-5, pp. 2056–2063, 2015.

[27] A. Shukla and S. P. Harsha, "Vibration response Analysis of Last stage LP turbine blades for variable size of crack in root," *Procedia Technology*, vol. 23, pp. 232–239, 2016.

[28] S. Zucca, T. Berruti, and L. Cosi, "Experimental and numerical investigations on the dynamic response of turbine blades with tip pin dampers," *Journal of Physics: Conference Series*, vol. 744, Article ID 012131, 2016.

[29] S. Quaegebeur, B. Chouvion, and F. Thouverez, "Nonlinear dynamic analysis of three-dimensional bladed-disks with frictional contact interfaces based on cyclic reduction strategies," *International Journal of Solids and Structures*, vol. 236-237, Article ID 111277, 2022.

[30] E. P. Petrov, "Method for sensitivity analysis of resonance forced response of bladed disks with nonlinear contact interfaces," *Journal of Engineering for Gas Turbines & Power*, vol. 131, no. 2, Article ID 022510, 2009.

[31] M. Krack, L. Salles, and F. Thouverez, "Vibration prediction of bladed disks coupled by friction joints," *Archives of Computational Methods in Engineering*, vol. 24, no. 3, pp. 589–636, 2017.

[32] A. Koscso and E. Petrov, "Sensitivity and forced response analysis of anisotropy-mistuned bladed disks with nonlinear contact interfaces," *Journal of Engineering for Gas Turbines & Power*, vol. 141, no. 10, Article ID 101025, 2019.

[33] J. J. Chen, C. P. Zang, B. Zhou, and E. P. Petrov, "Analysis of nonlinear modal damping due to friction at blade roots in mistuned bladed disks," *Journal of Engineering for Gas Turbines & Power*, vol. 143, no. 3, Article ID 031019, 2021.

[34] R. Z. Zhu, X. N. Zhang, S. G. Zhang, Q. Dai, Z. Qin, and F. Chu, "Modeling and topology optimization of cylindrical shells with partial CLD treatment," *International Journal of Mechanical Sciences*, vol. 220, no. 15, Article ID 107145, 2022.

[35] S. N. Zhao, L. F. Zhang, R. Z. Zhu, Q. Han, Z. Qin, and F. Chu, "Modeling approach for flexible shaft-disk-drum rotor systems with elastic connections and supports," *Applied Mathematical Modelling*, vol. 106, pp. 402–425, 2022.